SUPPORTING INFORMATION

MAGNETIC COUPLING AND SPIN ORDERING IN BISDITHIAZOLYL, THIASELENAZOLYL, AND BISDISELENAZOLYL MOLECULAR MATERIALS

C. Roncero-Barrero, J. Ribas-Ariño, I. de P.R. Moreira, M. Deumal

Secció Química Física, Dept. Ciència de Materials i Química Física,
and Institut de Química Teòrica i Computacional IQTCUB, Universitat
de Barcelona, Martí i Franquès, 1 - E08028 Barcelona

Section 1 - *Selection of A-B pairs of radicals (X-Ray 100 K and optimised 0 K crystal data) to evaluate the J_{AB} magnetic coupling*

The four bisDTA crystals studied (namely, (S,S), (S,Se), (Se,S) and (Se,Se) compounds according to the E_1/E_2 element substitution, see Figure S1.1) are isostructural and, excluding small differences in distances and tilting angles, present the same crystal packing.
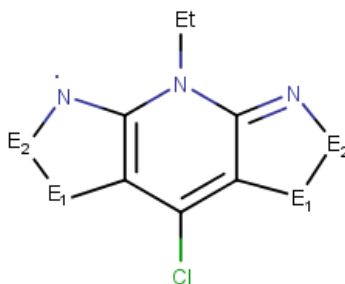

Figure S1.1. Radicals are classified according to whether E_1 and E_2 positions are S or Se atoms. In the following, radicals will be referred to as (E_1,E_2), namely, as pure bisdithiazolyl (S,S) radical, mixed thiaselenazolyl (S,Se) and (Se,S) radicals, and pure bisdiselenazolyl (Se,Se) radical.

Hereafter we describe the terminology used for all of them in order to name the selected radical···radical interactions, irrespective of the crystal data coming from either the X-Ray structure at 100 K or the optimised structure at 0 K. Taking a radical (identified as "central" in Figure S1.2) as reference, the *ab*-plane of the crystal shows five non-symmetry related π-stacks (namely, 1, 2, 3, 5 and 8 in Figure S1.2, which are highlighted in blue). Notice that π-stacks 4, 6 and 7 are equivalent to 2, 3 and 5, respectively. Further analysis shows that the interactions between "central-2" and "central-5" radicals are equivalent. From each π-stack, the 3 radicals closest to the central reference radical are referred as "#a", "#b" and "#c" where # stands for the number that identifies the stack (see Figure S1.2).
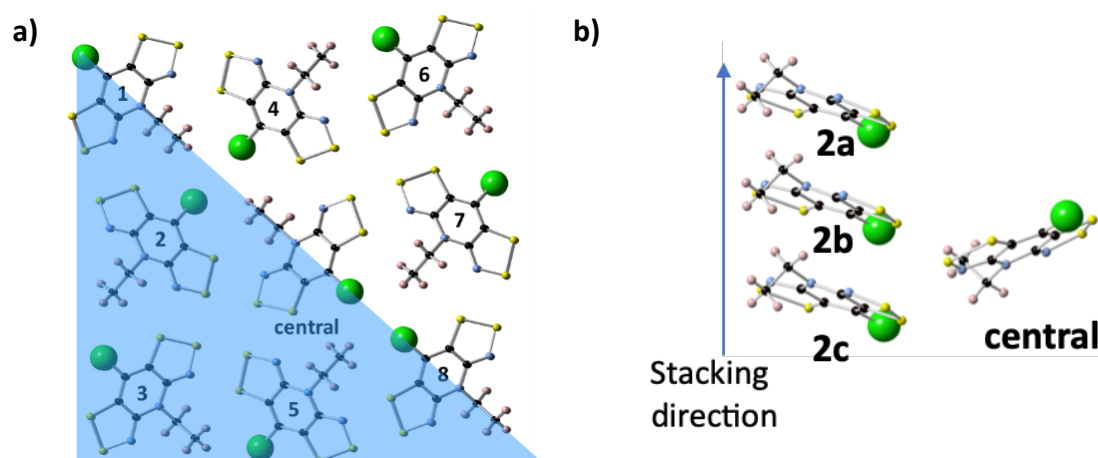

Figure S1.2. Selection of pairs of radicals that might be magnetically important. (a) View along the *ab*-plane (see region highlighted in blue for non-symmetry related π-stacks). (b) View along the π-stacking (*c*-axis) direction of the 3 dimers formed by the "central" reference radical and the radicals in the π-stack numbered "2".

Table S1.1 Exchange J_{AB} couplings (in cm^{-1}) computed at UB3LYP/6-311+G(d,p) level using the X-ray crystallographic data at 100 K, and the optimised crystal data at 0 K. Note that $E_2 \cdots E_2$ and shortest $E_2 \cdots E_1$ distances (in Å) between radicals are given. Also crystal orientation of all three radical pairs with significant J_{AB} interactions within the crystal is given (notice that a- and b-axes are equivalent due to P$\bar{4}2_1$m symmetry). Note that J_π, J_{2b} and J_{2c} stand for the magnetic exchange coupling between radicals along the π-stacking, Central-2b and Central-2c, respectively, in Figure S1.1.

System	Radical pair	orientation	Dist ($E_2 \cdots E_2$) / Å		Dist ($E_2 \cdots E_1$) / Å		J_{AB} /cm^{-1}	
			0 K	100 K	0 K	100 K	0 K	100 K
(S,S)	J_π	c-axis (π-stacking)	4.01	4.03	3.69	3.68	-1.45	-5.60
	J_{2b}	ac(=bc)-plane	3.40	3.49	3.25	3.52	3.73	0.01
	J_{2c}	$a(=b)$-axis	3.25	3.34	4.23	4.30	5.36	3.80
(S,Se)	J_π	c-axis (π-stacking)	3.95	4.02	3.74	3.74	7.77	0.30
	J_{2b}	ac(=bc)-plane	3.37	3.40	3.58	3.61	-2.11	0.35
	J_{2c}	$a(=b)$-axis	3.07	3.27	4.22	4.39	11.51	7.20
(Se,S)	J_π	c-axis (π-stacking)	4.09	4.09	3.74	3.68	-8.01	-12.40
	J_{2b}	ac(=bc)-plane	3.61	3.54	3.48	3.44	0.66	1.50
	J_{2c}	$a(=b)$-axis	3.17	3.40	4.16	4.36	7.19	3.40
(Se,Se)	J_π	c-axis (π-stacking)	4.09	4.13	3.81	3.78	2.22	-7.40
	J_{2b}	ac(=bc)-plane	3.49	3.46	3.60	3.58	-1.36	0.09
	J_{2c}	$a(=b)$-axis	3.20	3.36	4.40	4.53	8.67	5.60

A total of 13 dimers for each system have been selected, i.e. the pairs of radicals evaluated are central vs. 1a-c, 2a-c, 3a-c and 8a-c, and central vs. top (or bottom) radical to assess the π-stack (see Figure S1.2 for clear view of the dimers). Our calculations at UB3LYP/6-311+G(d,p) level show that only 3 pairs of radicals have non-negligible J_{AB} exchange interactions, namely the J_π magnetic coupling along the π-stacking, and in-plane J_{2b} and J_{2c} interactions. Comparison between relevant distances and J_{AB} magnetic couplings using crystallographic data at 100 K and optimised data at 0 K data is given in Table S1.1 . It is clear that the large sensitivity of J_{AB} to very small structural changes upon temperature is going to be decisive and lead to drastic changes in the magnetic response of a given bisDTA-derivative.

As mentioned above, J_{AB} is very sensitive to small structural changes upon temperature in all bisDTA-derivatives. Therefore, we would like here to digress to comment on the unit cell parameters selected as initial guess in the periodic geometry optimisation of all four bisDTA crystal packing. Due to the lack of low temperature experimental data, the cell parameters were extrapolated at 0 K from the data at 100 and 295 K reported in the literature (Robertson *et al. J. Am. Chem. Soc.*, 2008, **130**, 8414–8425). For (Se,Se), there is a recent crystal structure characterised at 2 K (Robertson et al. *Chem. Commun.* 2021, **57**, 10238–10241), and we will

next proceed to compare the unit cell parameters at 2 K with those obtained upon geometry optimisation at 0 K. we can compare

For (Se,Se), experimentalists observed a small contraction of the *c*-axis and an enlargement of the *a*- and *b*-axes when comparing unit cell parameters characterized at 100 K and at 2 K, which makes our predictions differ from the experiments by 0.03 Å referring to *c*-axis and 0.06 Å referring to *a*- and *b*-axes. Magnetic interactions along the stacking direction (*c*-axis) are the ones that present the largest variation upon optimization, since the AFM @100 K interaction becomes a FM @0 K interaction. Yet, we believe that the 0.03 Å difference in the *c*-axis parameter should not affect substantially the results. Thus the resultant J_{π} interaction is expected to appear near our 0 K predicted value in the magneto-structural correlation map (see white symbol in main text Figure 12b and Figure S1.3), irrespective of the initial values used for the optimisation being extrapolated cell parameters or experimentally determined at 2 K.
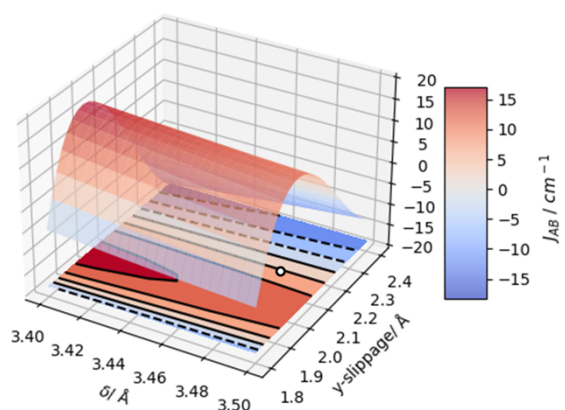

Figure S1.3. Magneto-structural correlation maps of a π-stacked pair of (Se,Se) radicals as a function of δ interplanar distance and latitudinal (y) slippage. Pair models have been constructed using the 0 K optimized monomer at PBE-D2 level. All J_{AB} are computed at UB3LYP/6-311+G(d,p) level. Note that value of J_{AB} magnetic coupling calculated using (Se,Se) radicals at 0 K (○) is placed in correlation map .

Section 2 - *Magnetic models to calculate magnetic susceptibility χT(T) data*

The energy spectrum for all four isostructural pyridine-bridged bisDTA-derivatives has been computed using a minimal magnetic model that accounts for all the relevant interactions by means of the Heisenberg Hamiltonian.

$$\hat{H} = \sum_{A>B} -2J_{AB}\hat{S}_A\hat{S}_B$$

where J_{AB} are the computed magnetic interactions discussed in Supporting Information Section 1. Note that a positive (negative) value of J_{AB} coupling corresponds to a ferromagnetic FM (antiferromagnetic AFM) interaction.

Two magnetic models containing 16 radical centres and accounting for the most important magnetic interactions have been tested in order to explored which magnetic model extracted from the 3D magnetic topology of (S,S), (Se,S) and (Se,Se) at 100 and 0 K, and (S,Se) at 0 K offers the most realistic description of their magnetic behaviour (see Figure S2.1). Firstly, a 16-radical model constructed elongating the unit cell along the *c*-axis is selected to consider the importance of the π-stacking interaction. Secondly, a 16-radical model extended along the *a*-axis (which is equivalent to the *b*-axis) is chosen to be able to consider the cooperativity of the magnetic interactions along the *ab*-plane. For (S,Se) at 100 K, a 2D magnetic model was used instead since the magnetic topology was found to be 2D (see Figure S2.2).
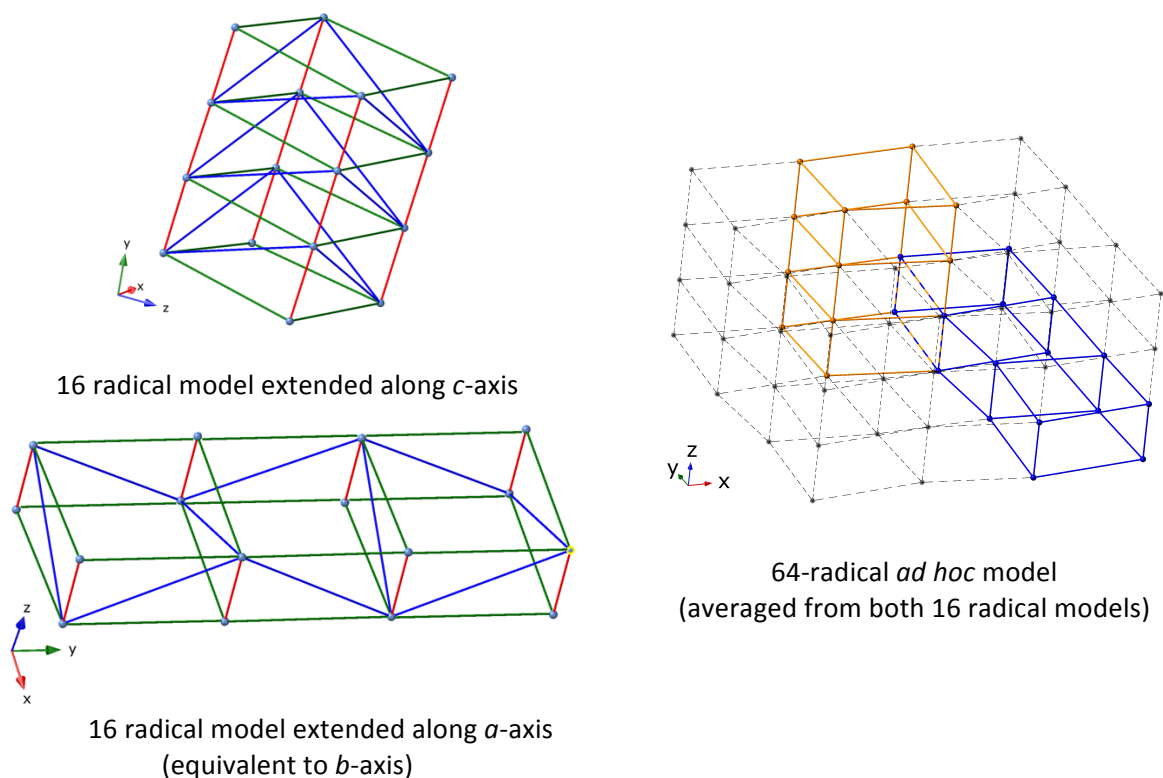

16 radical model extended along *c*-axis

16 radical model extended along *a*-axis
(equivalent to *b*-axis)

64-radical *ad hoc* model
(averaged from both 16 radical models)

Figure S2.1 Magnetic models used to describe (S,S), (Se,S) and (Se,Se) at 100 and 0 K, and (S,Se) at 0 K.
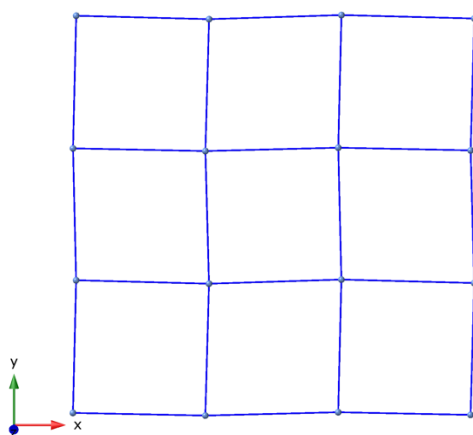
Figure S2.2 Magnetic model of (S,Se) at 100K

Table S2.1 bisDTA g-factors employed in the simulations, obtained from Robertson *et al. J. Am. Chem. Soc.* **2008**, *130*, 8414–8425.

	(S,S)	(S,Se)	(Se,S)	(Se,Se)
g-factor	2.0082	2.0111	2.0190	2.0284

By means of statistical mechanics, using the canonical partition function constructed with the previously computed energy spectra, the macroscopic magnetic susceptibility at zero-field limit is computed as:

$$\chi = \frac{N_A g^2 \mu_B^2}{k_B T} \mu_o \left[\frac{\sum_n S_n(S_n+1)(2S_n+1)e^{\left[\frac{-(E_n-E_o)}{K_B T}\right]}}{\sum_n (2S_n+1)\, e^{\left[\frac{-(E_n-E_o)}{K_B T}\right]}} \right]$$

where N_A is the Avogadro number, g is the gyromagnetic constant, μ_B is the Bohr magneton, k_B is the Boltzmann constant, and E_0 and S_0 are the energy and the spin of the ground state, respectively. Note that the g-factor used for each bisDTA compound is listed in Table S2.1.

Magnetic susceptibility χT(T) data calculated using J_{AB}(X-Ray data at 100 K) for (S,S) and (Se,S) using both 16-radical magnetic models, extended along *a*- or *c*-axes, follow adequately the experimental paramagnetic and spin-canting antiferromagnetic tendencies, respectively (see Figure S2.3). In addition, an *ad hoc* 64-radical magnetic model has been put forward from averaging the χT(T) data obtained using the two 16-radical magnetic models aforementioned, which gives a proper estimation of the cooperativity effect of all three significant magnetic couplings in (S,S) and (Se,S) compounds.
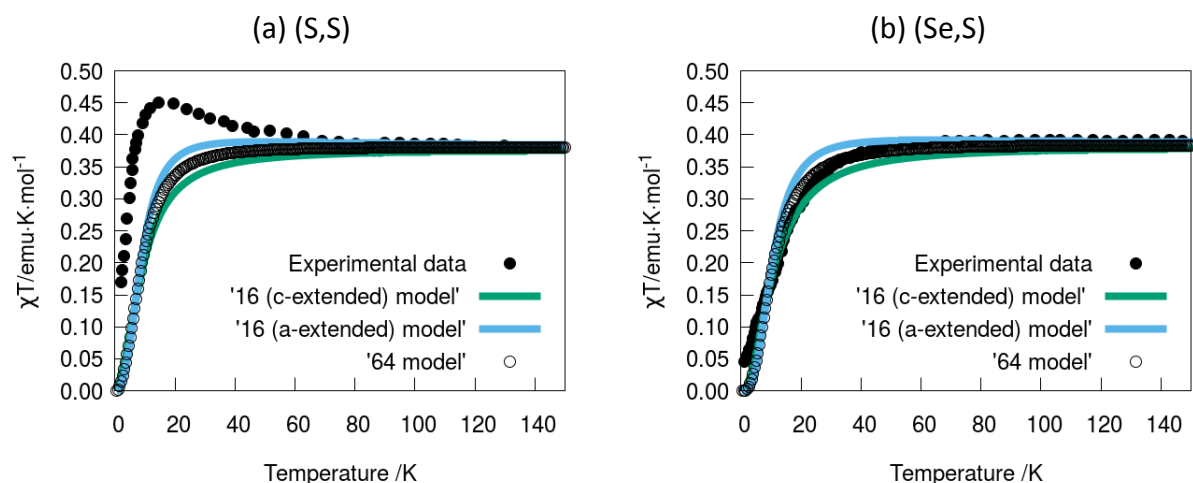
Figure S2.3. Magnetic susceptibility χT(T) calculated using J_{AB}(X-Ray data) for (a) (S,S) and (b) (Se,S) using both 16-radical magnetic models, extended along *a*- or *c*-axes, and the *ad hoc* 64-radical magnetic model (see Figure S2.1) made from averaging the χT(T) data obtained using the two aforementioned 16-radical magnetic models.
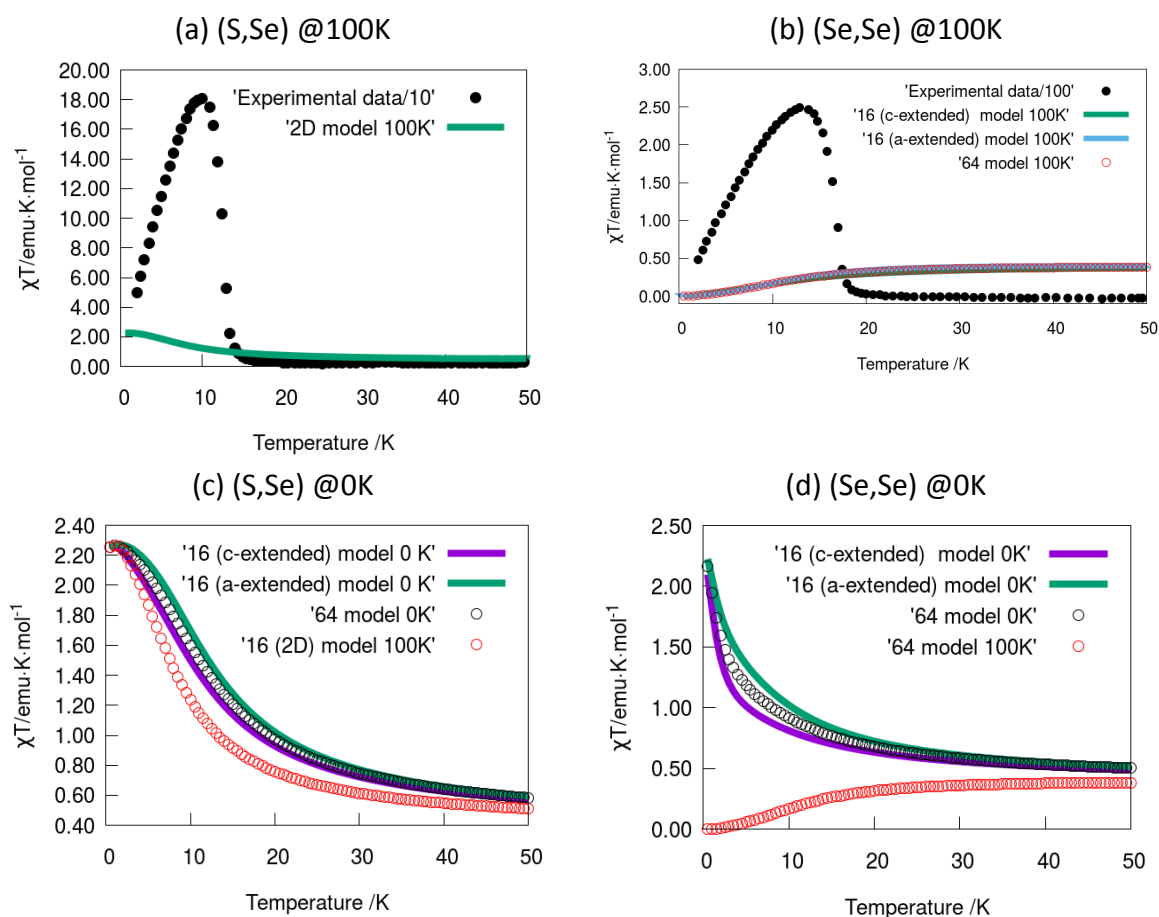

Figure S2.4. Magnetic susceptibility χT(T) calculated using data at 100 K (X-Ray data, top row), and at 0 K (optimised data, bottom row) for (S,Se) and (Se,Se).

Same magnetic susceptibility $\chi T(T)$ calculation using J_{AB}(X-Ray data at 100 K) for (S,Se) and (Se,Se) using both 16-radical magnetic models, extended along both *a*- and *c*-axes, failed dramatically to describe the experimental bulk ferromagnetic behaviour of these two compounds (see Figure S2.4a-b). In this case, it is necessary to resort to crystal data obtained at 0 K after periodic geometry optimisation to achieve bulk ferromagnetic $\chi T(T)$ data (see Figure S2.4c-d). However, although the calculated $\chi T(T)$ data shows a clear ferromagnetic response, it does not show the experimental $\chi T(T)$ maximum value of *ca.* 200 emu·K·mol^{-1} , whose realisation would certainly require a FM J_{AB} interaction at least two orders of magnitude larger than both our calculated magnetic couplings and those reported in the literature for these bisDTA compounds [Robertson *et al.*, *Chem. Commun.* **2021**, *57*, 10238–10241].

Section 3 - *SOMO and spin density of bisDTA radicals*

The singly occupied molecular orbital (SOMO) of (S,S), (S,Se), (Se,S) and (Se,Se) obtained at UB3LYP/6-311+G(d,p) level has clearly the same contribution from the π-system of S and/or Se heteroatoms (see Figure S3.1). In addition, the spin density for all four bisDTA compounds computed at the same level of theory also shows the same contribution coming from the same atoms, irrespective of being S or Se (see Figure S3.2).
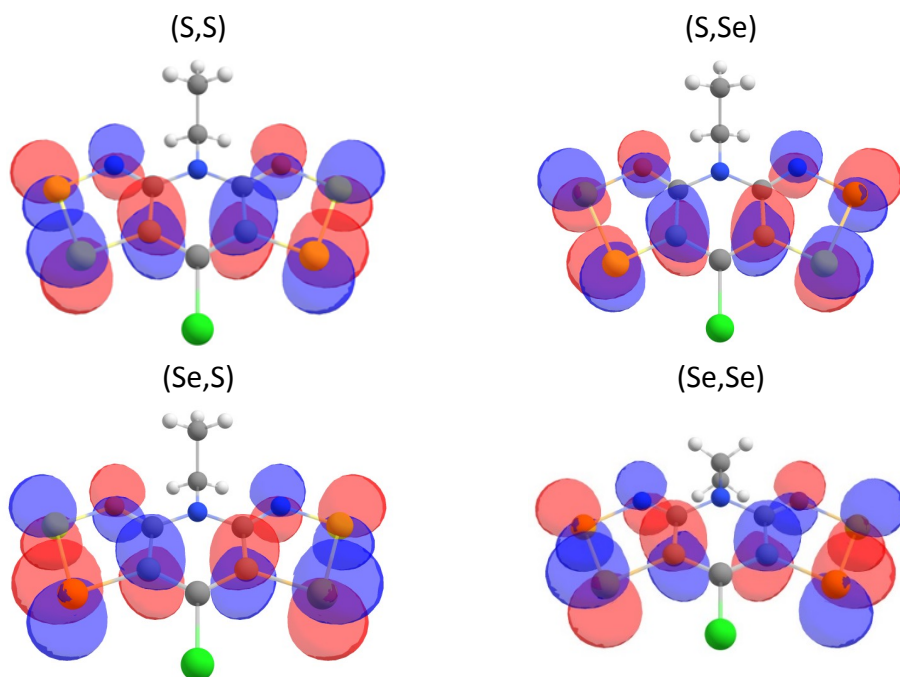
(S,S) (S,Se)

(Se,S) (Se,Se)

Figure S3.1. Singly occupied molecular orbital (SOMO) for (S,S), (S,Se), (Se,S) and (Se,Se) radicals.
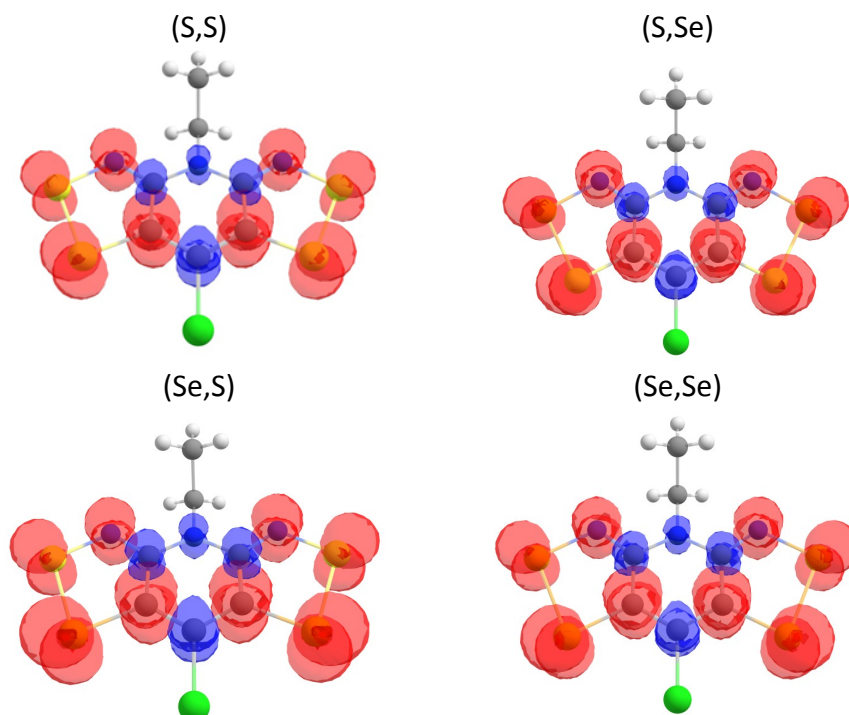
(S,S) (S,Se)

(Se,S) (Se,Se)

Figure S3.2. Spin density of (S,S), (S,Se), (Se,S) and (Se,Se) calculated at UB3LYP/6-311+G(d,p) level.

Section 4 - *On the deviation between experimental and calculated χT(T) data of (S,S)*

We would like to remark that, among all four isostructural bisDTA-derivatives, (S,Se) and (Se,Se) are the most interesting from both magnetic and computational points of view because they behave as a bulk ferromagnet, while (S,S) shows no long-range magnetic order and (Se,S) exhibits canted antiferromagnetism. Therefore, we devoted our efforts to fully understand both (S,Se) and (Se,Se) bulk ferromagnets. As for (S,S) and (Se,S), our calculated J_{AB}'s could reproduce their main magnetic features, and our study did not aim at quantitatively reproduce the experimental χT(T) data for (S,S). Yet, we analysed in full detail our data to be certain we had captured adequately the magnetic behaviour of (S,S), namely, in terms of (1) J_{AB} magnetic couplings, and (2) relative error between experimental and calculated χT(T) data.

First of all, as had been suggested by experimentalists (Robertson *et al.*, *J. Am. Chem. Soc., 2008*, **130**, *8414–8425*), at low temperature there is a competition between FM and AFM interactions which is actually said to be the origin of the maximum at 15 K exhibited by experimental χT(T) data. Our calculations show indeed that there is a competition between -5.6 cm^{-1} AFM and +3.8 cm^{-1} FM couplings at 100K, as shown in main text Figure 5a. The competition is shown to be preserved upon optimisation at 0 K (-1.5, +3.7 and +5.4 cm^{-1} in main text Figure 7a).
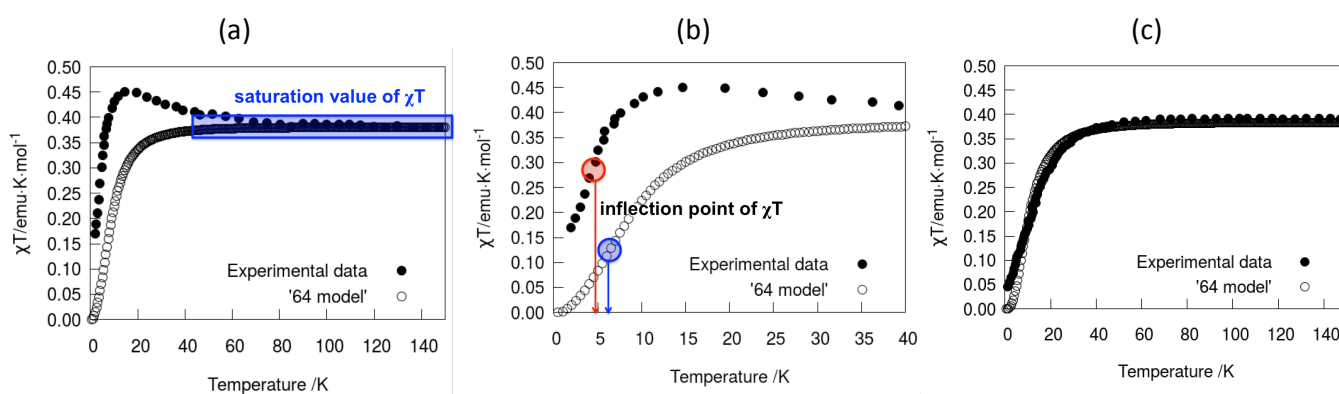

Figure S4.1. Magnetic susceptibility χT as a function of temperature for (S,S) ranging from 0 to (a) 150 K and (b) 40 K, and (c) for (Se,S) ranging from 0 to 150 K.

Referring to the relative error between experimental and calculated χT(T) data, it is first worth mentioning that the 0 to 150 K temperature range selected in Figure S4.1a (which actually is main text Figure 6a) accentuates the height of the maximum at 15 K of experimental χT(T) compared to calculation. This visual effect can be easily realized when comparing Figures S4.1a and S4.1b. Please be aware that we are not denying the existence of the maximum, we are stressing the fact that, although numerical agreement is not reached, the shape of calculated and experimental curves follows the same tendency (see Figure S4.1b). Secondly, in addition to general resemblance, analysis of the inflection point in both cases shows that it is reached at approximately the same temperature, as indicated in Figure S4.1b. Once more the behaviour of calculated and experimental data is very similar. At this

point, one has to keep in mind that the value of all computed J_{AB} magnetic couplings between radicals is of the order of units of wavenumbers. It thus follows that a difference of 0.20 emu K mol^{-1} is actually numerically not very relevant since, again, the shape of both curves is much the same. All-in-all, we were not troubled with our simulated data not overlapping the experimental data for (S,S), and did not pursue any further studies on that compound. Actually, from our own perspective, the complete agreement between experimental and calculated data for (Se,S) deserves to be acknowledge (see Figure S4.1c), since it awkwardly highlights that the data for (S,S) slightly deviates when cooling down from 40 K.

Section 5 - *Spin correlation for (S,Se) compound*

The representation of short- and long-range spin correlation for the (S,Se) thiaselenazolyl system shows a ferromagnetic ordered ground state using both experimental X-Ray geometry at 100 K and optimised PBE-D2 geometry at 0 K (see Figure S5.1). The main difference is that the magnetic topology is low dimensional (2D) at 100 K, whereas it is three-dimensional (3D) at 0 K. Despite the presence of weak AFM inter-stack J_{AB} at 0 K (J_{2c} = -2.1 cm^{-1}), the (S,Se) system presents a global FM ordering due to the propagation of short- and long-range interactions along all three crystallographic directions.
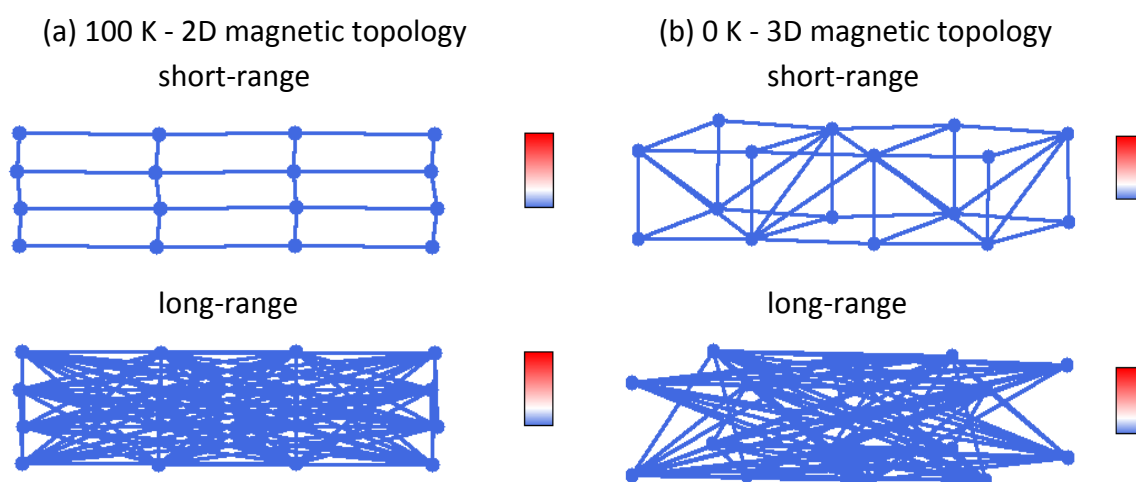
(a) 100 K - 2D magnetic topology
short-range

(b) 0 K - 3D magnetic topology
short-range

long-range

long-range

Figure S5.1. Short- and long-range spin exchange density matrix elements, P_{ij}, of the ground state for (S,Se) system obtained using (a) X-Ray data at 100 K for a 2D magnetic topology, and (b) optimised data at 0 K for a 3D magnetic topology. Colour codes for the sign of the interaction: blue means FM spin alignment and red stands for AFM alignment. Intensity of colour represents the strength of the interaction.

Section 6 - *Magneto-structural correlations*

Evaluation of the dependence of the magnetic interaction along the π-stacking on the slippage along x- and y-axes and interplanar distance between two π-stacked radicals was performed using a dimer extracted from the (1) X-Ray (100 K) and (2) PBE-D2 optimised (0 K) geometries (see Figure S6.1 and Table S6.1 for slippage and distance). Analysis of the extracted radical pairs from a top view (see Figure S6.2 for dimers at 100 K, and Figure S6.3 for pairs at 0 K) shows that the systems do not exhibit latitudinal slippage at any temperature, and that from direct observation no significant differences can be realised. Therefore, in order to understand the key structural parameters that explain the temperature effects, we re-explore the (Se,Se) correlation map reported in the literature (Leitch *et al. J. Am. Chem. Soc.* **2009**, *131*, 7112) accounting for longitudinal y-slippage and interplanar (δ) distance parameters.
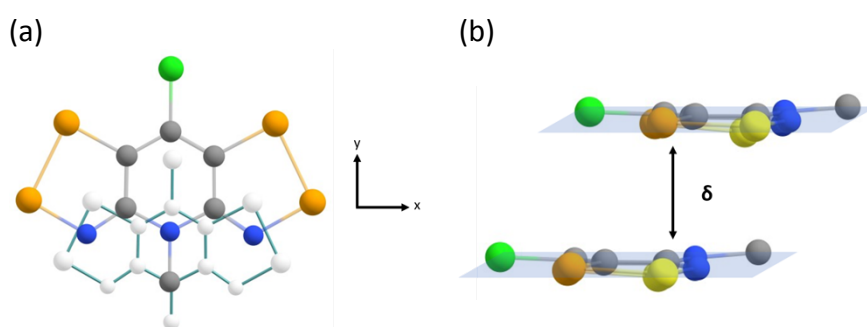

Figure S6.1. (a) Representation of a dimer along the π-stacking direction showing longitudinal and latitudinal slippages (along x- and y-axis, respectively). Ethyl substituent has been omitted for simplification. Bottom monomer in white for contrast and visualization purposes. (b) Pair of bisDTA radicals piled up at a δ interplanar distance at the π-stacking

Table S6.1 y-slippage and δ (in Å) before (100 K) and after (0 K) optimisation.

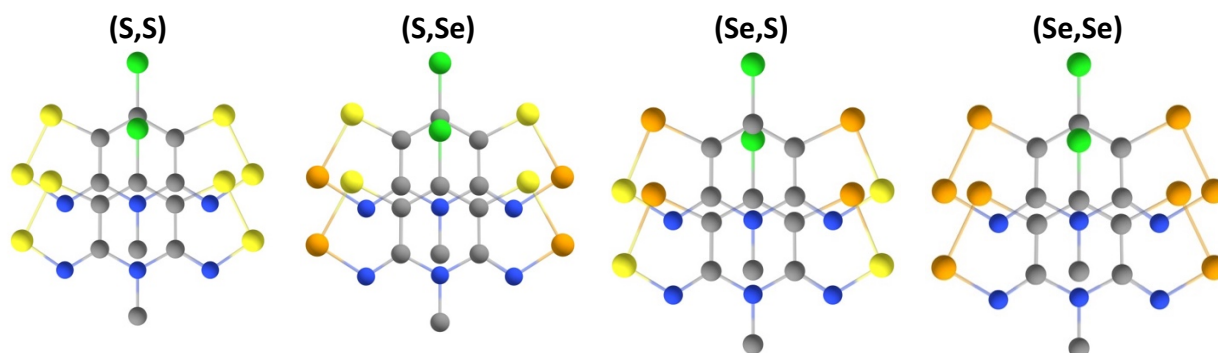|	(S,S)		(Se,S)		(S,Se)		(Se,Se)	
	100 K	0 K	100 K	0 K	100 K	0 K	100 K	0 K
δ / Å	3.42	3.47	3.46	3.38	3.41	3.37	3.49	3.48
y-slippage/ Å	2.13	2.11	2.17	2.08	2.11	2.04	2.2	2.19

Figure S6.2 Representation of dimers along the π-stacking for all four bisDTA compounds extracted from the crystallographic data at 100K [Robertson *et al. J. Am. Chem. Soc.*, **2008**, 130, 8414].
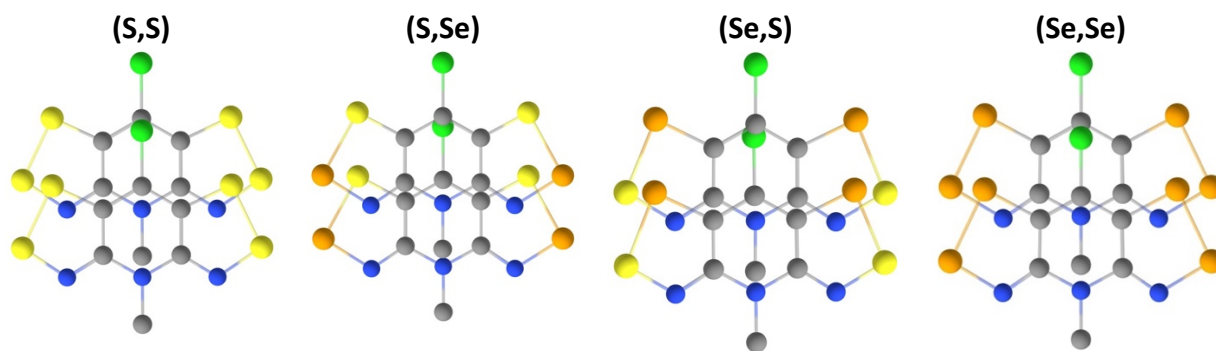
Figure S6.3 Representation of dimers along the π-stacking for all four bisDTA compounds extracted from the PBE-D2 optimised crystals.
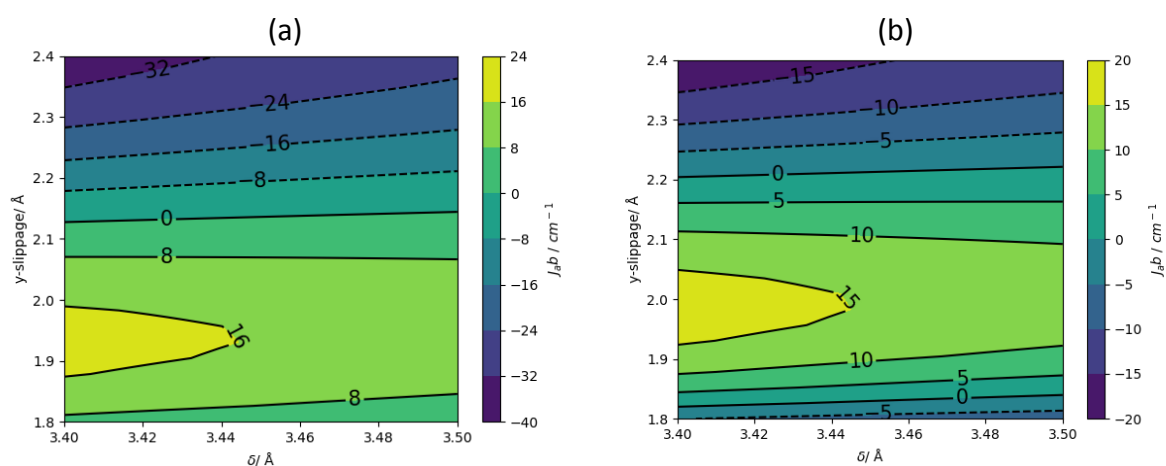

Figure S6.4 Contour plots of (Se,Se) dimers constructed with a monomer extracted from (a) X-Ray (100 K) structure, and (b) optimised structure (0 K)
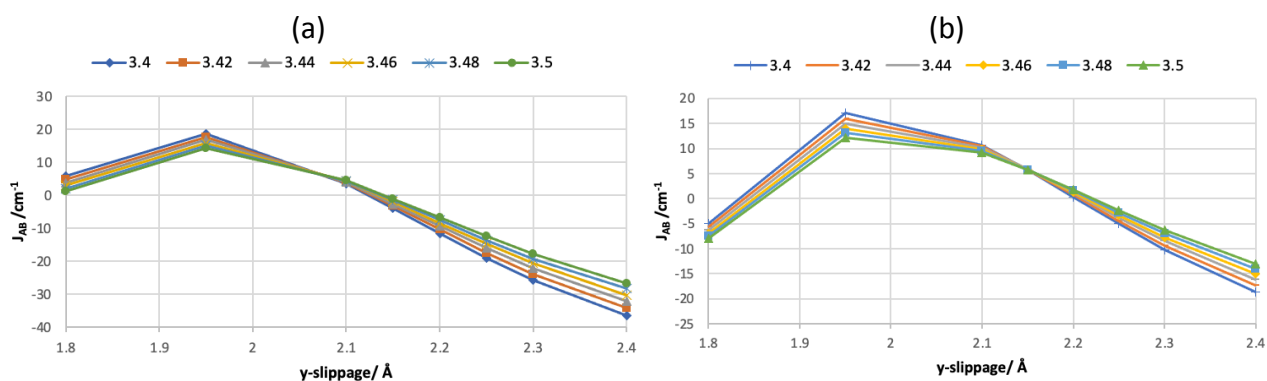

Figure S6.5 Projections at constant δ of the (Se,Se) correlation maps using (a) X-Ray and (b) PBE-D2 optimised data.

The resultant (Se,Se) contour plots show that J_π interaction can change from AFM to FM (and *vice versa*) due to small variations in δ and longitudinal slippage (see Figure S6.4). For both 100 K and 0K cases, FM regions appear at small values of y-slippage. However, in the contour plot constructed with a radical pair extracted from the 0 K optimised structure, J_{AB}=0 isolines appear earlier, at larger values of slippage (~2.21Å), and it becomes AFM again around 1.83 Å (compare Figures S6.4a and S6.4b). This shift of the FM region evidences the J_π dependency on not just y-slippage and δ intermolecular parameters, but also on the intra-monomer geometry. Note that the contour plots show that J_π exhibits a small dependence on δ in the analysed range (see projections at constant δ represented in Figure S6.5), and that the AFM/FM transition is slightly affected by δ.